The physics of tokamak start-up

D. Mueller

Citation: Phys. Plasmas **20**, 058101 (2013); doi: 10.1063/1.4804416
View online: http://dx.doi.org/10.1063/1.4804416
View Table of Contents: http://pop.aip.org/resource/1/PHPAEN/v20/i5
Published by the American Institute of Physics.

The physics of tokamak start-up[a)]

D. Mueller[b)]
Princeton Plasma Physics Laboratory, P.O. Box 451 Princeton, New Jersey 08543, USA

(Received 12 December 2012; accepted 14 March 2013; published online 10 May 2013)

Tokamak start-up on present-day devices usually relies on inductively induced voltage from a central solenoid. In some cases, inductive startup is assisted with auxiliary power from electron cyclotron radio frequency heating. International Thermonuclear Experimental Reactor, the National Spherical Torus Experiment Upgrade and JT60, now under construction, will make use of the understanding gained from present-day devices to ensure successful start-up. Design of a spherical tokamak (ST) with DT capability for nuclear component testing would require an alternative to a central solenoid because the small central column in an ST has insufficient space to provide shielding for the insulators in the solenoid. Alternative start-up techniques such as induction using outer poloidal field coils, electron Bernstein wave start-up, coaxial helicity injection, and point source helicity injection have been used with success, but require demonstration of scaling to higher plasma current. © *2013 AIP Publishing LLC*. [http://dx.doi.org/10.1063/1.4804416]

I. INTRODUCTION

This paper describes the physics of the start-up phase of tokamak operation. Recent experience on the start-up of the Experimental Advanced Superconducting Tokamak (EAST),[1] the Korean Superconducting Tokamak Advanced Research (KSTAR),[2] and start-up experiments in the Joint European Torus (JET)[3] with the International Thermonuclear Experimental Reactor (ITER)-like-wall (ILW)[4] provides a perspective for planning for the start-up of the National Spherical Torus Experiment Upgrade (NSTX-U),[5] the Japan Torus 60-Super Advanced (JT-60SA),[6] and the ITER,[7] which will be carried out in the coming years. These devices will rely upon a central solenoid for start-up. However for long pulse spherical tokamaks (STs), non-central solenoidal start-up is very important and it is essential for an ST reactor. The leading techniques for start-up without a central solenoid in an ST include outer poloidal field coil start-up[8,9] Electron Bernstein Wave start-up[10] and helicity injection form Coaxial Helicity Injection (CHI)[11] or from local helicity injection[12] by means of plasma guns.

II. INDUCTIVE START-UP

In present day tokamaks, the main technique to initiate breakdown and drive a toroidal current is use of a central solenoid that supplies magnetic flux and induces a toroidal electric field. Central solenoid start-up can be divided into three phases, the breakdown or avalanche phase, the impurity burn-through phase, and the controlled plasma current ramp-up, which will now be described. Typically, before start-up, hydrogen or deuterium gas is injected into the vacuum vessel and the solenoid is precharged with a current in the desired direction of the plasma current. The solenoid current is then driven toward zero by the action of power supplies, assisted by a resistive voltage in the coil and the external circuit. $V_{coil} = V_{ps} - I_{coil}R_{coil+}$, where V_{ps} denotes the applied power supply voltage, V_{coil} is the voltage on the coil, I_{coil} is the current in the coil, and R_{coil+} is the resistance of the coil, leads and any additional resistance that is inserted into the circuit. The one-turn loop voltage applied is given by $V_{loop} = V_{coil}M/L$, where M is the mutual inductance between the coil and the plasma and L is the inductance of the coil. The electric field at the radius R is $E = V_{loop}/2\pi R$.

A. Breakdown and avalanche

Some free electrons are almost always present in a tokamak chamber, but can be supplemented by radiation, heated filaments, or RF waves. These are accelerated by the electric field. If an electron gains over 13.6 eV before suffering a collision with a neutral atom, it can ionize the neutral atom and leave two electrons, which can be accelerated by the electric field and produce more subsequent electrons. Figure 1 shows the ionization cross-section of neutral hydrogen by electrons as a function of electron energy from Gryzinski's classical model.[13] Note the cross-section vanishes below 13.6 eV and peaks at about 50 eV and falls at higher energy. This process is known as the Townsend avalanche and is named after John Sealy Townsend.[14] If an electron produces α electrons per meter, then $dn_e = \alpha\, n_e\, dx$, where n_e is the density of electrons and x is the distance along the electric field direction.[15] An exponential growth in n_e occurs $n_e = n_e(0)\, e^{\alpha x}$, where α is called the first Townsend coefficient. The Paschen curve that describes the breakdown voltage of a gas between parallel plates for hydrogen is shown in Figure 2.[16] In order to minimize the loop voltage required and thereby reduce the hardware demands, there is an optimal product of pressure times distance of a few Torr-cm for breakdown in hydrogen. For a tokamak, the voltage is V_{loop}, the distance is $2\pi R$, and the pressure, p, can be chosen to be near the minimum in the Paschen curve to minimize hardware demands. The first

[a)]Paper UT3 1, Bull. Am. Phys. Soc. **57**, 340 (2012).
[b)]Invited speaker.

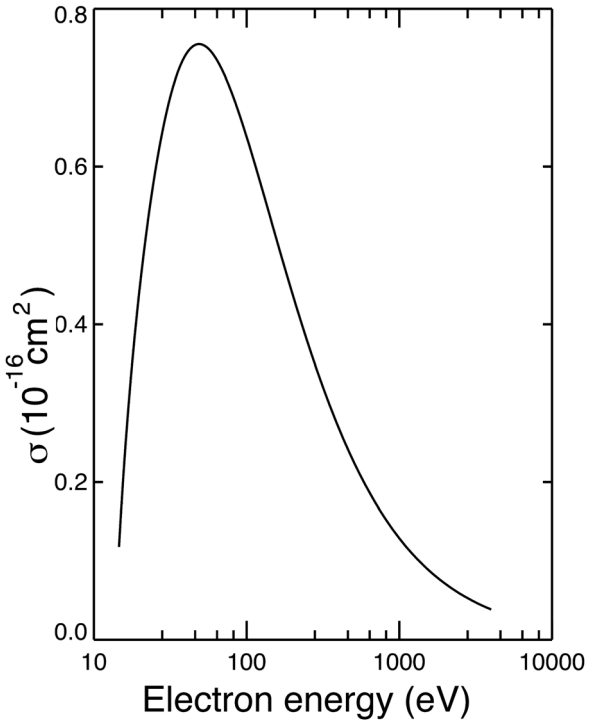

FIG. 1. The neutral hydrogen total ionization cross-section versus electron energy. Note that σ vanishes below 13.6 eV peaks near 30 eV and then decreases.

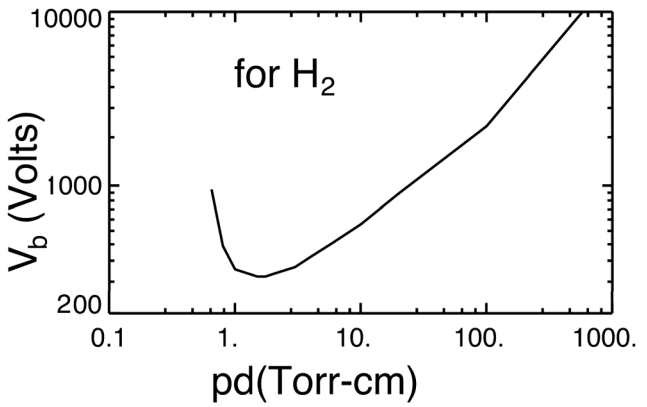

FIG. 2. The Paschen curve of breakdown voltage, V, between parallel plates separated by a distance d at pressure p for hydrogen. Note that there is a minimum pd for which breakdown occurs and above that minimum, V increases approximately linearly such that for fixed separation E/p is approximately constant.

Townsend coefficient, α, is not a simple function of E/p, but α/p is as is shown in Figure 3. As an example, for NSTX, $p \sim 5 \times 10^{-5}$ Torr and $V_{loop} \sim 2$ V/turn, $\alpha \sim 10^{-2}$/m, so the path length for which electrons must be confined before being lost must be >100 m, i.e., many toroidal transits. If the pressure is too high, the electrons will not gain enough energy to ionize the neutrals before elastic scattering changes their direction so that the electric field slows them. If the pressure is too low, the density of neutrals will not be sufficient to provide electrons for the avalanche to proceed. Typically, if the pressure is within about a factor of 2 from the optimum (in either direction) value, the avalanche will proceed. If the electrons are lost faster than the avalanche proceeds the avalanche will fail.

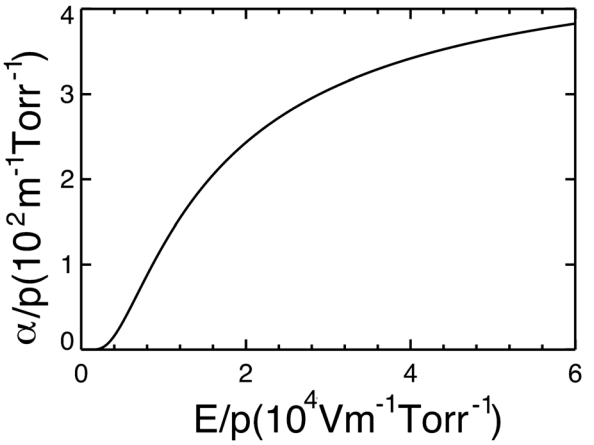

FIG. 3. The number of new electrons per unit length of path for an electron in a gas, the first Townsend coefficient, α is not a simple function E/p, but α/p is.

B. Impact of error fields

We consider electron losses parallel and perpendicular to the magnetic field separately. Under the influence of the induced toroidal electric field, electrons drift along the magnetic field that is predominantly in the toroidal direction. The electrons are subject transverse drifts due to the curvature of the field, its radial gradient and perpendicular fields generated by the poloidal field system and by eddy currents induced in surrounding conducting structures. Although the startup phase of each tokamak is designed to produce a localized, transient null in the poloidal field at the desired location of breakdown at the time of breakdown, in practice, there are always transverse fields surrounding the field null which evolve in time, and these generally dominate the transverse drifts of the electrons during startup so that after many transits, the electrons will impinge on the wall. For an average stray field $\langle \delta B \rangle$, the connection length to the wall, L is about $h \bullet B_T / \langle \delta B \rangle$ where B_T is the toroidal field and h is the typical transverse distance to the wall of the device. For NSTX, $\langle \delta B \rangle$ is 2.5 to 5 G so L is about 3000 m, much longer than the 200 m ionization length under typical inductive startup conditions.

During the avalanche phase, the average electron drift velocity v_{de} parallel to the field is approximately 35 E/p (m/s) so the time for electrons to drift to the wall is about 6 ms. For ions, $v_{di} \sim 0.9$E/p (m/s) and the time to drift to the wall is ~150 ms, so secondary emission is unimportant during the avalanche. Lloyd[17] estimates the time to complete the avalanche process to be $41/v_{de}$ (α-L^{-1}), which is 7 ms for NSTX parameters.

For $E/p > 5 \times 10^3$ $Vm^{-1}Torr^{-1}$, the electron temperature, T_e, is high enough that thermal ionization is important. Energy loss of the electrons in the ionization process limits T_e to below 10 eV until ionization of the initial gas is nearly complete[18] so $v_D \sim 4$ to 40 m/s and the loss time is 25 to 250 ms greater than the avalanche time for NSTX. Over a wide range of devices, $V_{loop} = 2$ to 30 V/turn, E = 0.3 to 2 V/m, $p = 10^{-5}$ to 10^{-4} Torr, and E/p = 0.4 to 3×10^4 $Vm^{-1}Torr^{-1}$. For JET,

Tanga found for $V_{loop}XB_T/\langle\delta B\rangle > 10^3$ V/m that the error fields were small enough and the loop voltage was high enough that the avalanche could proceed.[19] The avalanche proceeds until electron-ion collisions dominate the process compared to electron-neutral collisions. The electron-ion and electron-neutral collision rates are equal when $n_e \sim 0.1\ n_0$. The current density, $j = \gamma\ n_0\ e\ v_{de}$, where γ is the H or D ionization fraction is 15 to 40 kA/m^2, which corresponds to a plasma current, I_p, of 5 to 10 kA for NSTX and about 20 kA for JET. For $I_p = 10$ kA and a plasma minor radius of 0.5 m, the poloidal field at the edge of the plasma is about 40 G, comparable to the stray fields. At the end of the avalanche phase, $\gamma = 0.5$, Coulomb collisions dominate but until ionization is nearly complete, T_e is limited to below 10 eV.

C. Burn-through

The burn-through phase begins at the end of the avalanche. In this phase, low-Z impurities, usually originating from the walls surrounding the plasma column, radiate and can limit the temperature and the current ramp-rate so that the discharge fails. The radiated power density, P_{Rad}, is given by $n_e \Sigma n_Z f(Z,T_e)$, where n_Z is the impurity density, f(Z,Te) is the cooling rate from impurities,[20] and the sum is over the impurity species. Figure 4 shows the steady state cooling rate due to impurity radiation from Be, C, and O as a function of T_e. Note that the cooling rate for Be is 10 times less than for C or O. Also it is important to note that the peak cooling occurs at about 8 and 20 eV for C and O, respectively. The power available to support the radiation is limited by the power supplies to E^2/η at low T_e and by $j^2\eta$ at high T_e, where η is the plasma resistivity. There must be some power left over to increase I_p and heat the plasma or the discharge will cool and collapse. The lower sputtering yield for high-Z materials at low plasma temperature make them less important at start-up. In order to facilitate burn-through, various techniques have been employed. Wall conditioning can reduce the influx of low-Z materials. High temperature bakeout removes hydrocarbons and water from graphite.[21] Higher surface temperatures accelerate this removal and temperatures of at least 300 °C are usually required for effective bakeout. Helium Glow Discharge Cleaning (HeGDC) removes hydrogen and deuterium and water from the graphite surface.[22] Boronization or other surface coatings using various application techniques reduces oxygen impurities.[23] Lithium coatings can reduce the influx of C, O, and H/D.[24] The use of metal walls can reduce the source of low-Z impurities compared to graphite walls.[25] Auxiliary heating can be used to increase the power available to burn through the low-Z radiation.

Recent modeling of the avalanche and burn-through phases by H-T Kim[26] of JET start-up agrees well with experiment. This model uses deuterium confinement time τ_D from $1/\tau_D = 1/\tau_{D,\parallel} + 1/\tau_{D,\perp}$ where $\tau_{D,\parallel}$ and $\tau_{D,\perp}$ are the confinement times due to parallel and perpendicular losses. The parallel distance traveled before loss, L(t), is a function of time since as the $I_p(t)$ increases the plasma's poloidal field becomes larger than the stray poloidal field. Kim uses $L(t) = 0.25 \bullet a(t) \bullet (B_T/\langle\delta B_z(t)\rangle) \bullet \exp(I_p(t)/I_{ref})$ with $I_{ref} = 100$ kA for JET. The confinement time due to parallel loss $\tau_{D,\parallel} = L(t)/C_s$, where C_s is the sound speed $((T_e + T_i)/m_D)^{1/2}$. The confinement time due to perpendicular losses $\tau_{D,\perp} = a(t)/v_{Bohm}(t)$ where $v_{Bohm}(t) = 2D_{Bohm}(t)/a(t)$ and $D_{Bohm}(t) = T_e(eV)/16B_T$. A dynamic recycling coefficient is used for deuterium while physical sputtering and a simple chemical sputtering yield are used for C and O. This self-consistent model matches the experimental time history of the start-up well, particularly for I_p, radiated power, carbon impurity radiation emission, and T_e.

Experimental results from JET with the ITER-like wall, ILW, permit comparison of start-up conditions with graphite walls compared to the new Be and W surfaces.[27] The results indicate that the density behavior is different for the ILW and the graphite wall at the time of burn-through. For the ILW, the density scales linearly with the prefill gas pressure, whereas for the graphite wall, the density varies with the prefill pressure, but with some additional amount due to recycling from the carbon wall. Also, the radiated power at the time of burn-through is a steep function of density for the carbon wall but weakly dependent on density for the ILW. The latter point is likely due to the much reduced radiative cooling from Be compared to C as seen in Fig. 4 as well as chemical sputtering of C from the graphite wall. Furthermore, on JET with the ILW, there were no failures of the start-up during the burn-through phase or failures due to deconditioning events, such as disruptions or excessive gas puffing on the previous shot, unlike with the graphite wall.

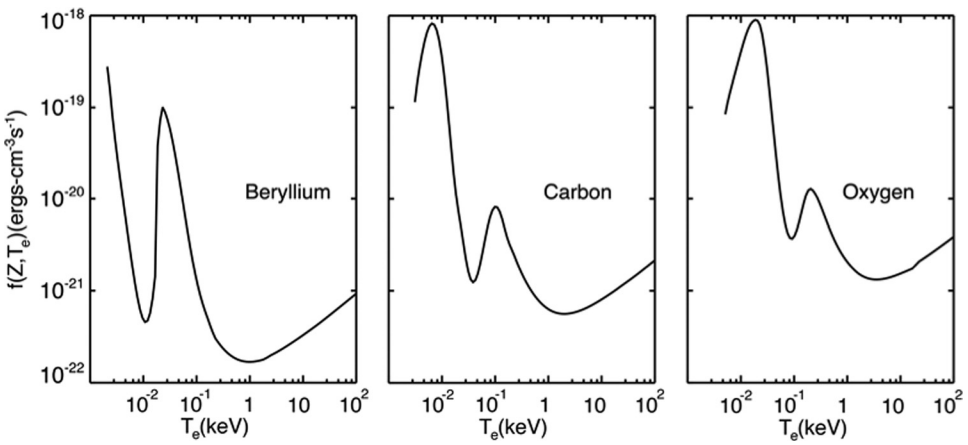

FIG. 4. The cooling rate due to impurity radiation, assuming coronal equilibrium is plotted as a function of electron temperature peaks below 20 eV for low Z impurities.

D. Additional requirement for tokamaks with superconducting coils

Fully superconducting tokamaks have limited loop voltage due to power supply cost, eddy-current heating in the coils and the need to limit induced currents in the cryostat and thick vacuum vessel. For ITER, the design value for the maximum electric field at start-up, $E \sim 0.3$ V/m, is at the lower limit of successful breakdown observed with purely inductive start-up in existing tokamaks. For example in EAST, the maximum electric field that can be applied using the power supplies alone is about 0.2 V/m, below the value needed for successful inductive start-up. Both EAST and KSTAR employ circuits that allow resistors to be switched in to each of the poloidal field coil circuits for a short time, in effect raising R_{coil} discussed in the beginning of Sec. II to produce a higher voltage for breakdown after the coils are charged to their initial magnetization states. Note that the voltage drop across the resistors increases the applied voltage in the direction to decrease the magnitude of the coil currents. Both of the operating fully superconducting tokamaks have less inductive power to heat the plasma and ramp the plasma current compared to conventional tokamaks due to their lower coil power supply voltage capabilities. The use of electron cyclotron radiofrequency heating (ECRH) has been demonstrated on a variety of tokamaks to lower the electric field required for breakdown by about a factor of about two.[17] Furthermore, ECRH can provide power to the plasma during burn-through when the plasma current is low and other heating methods, particularly inductive and energetic neutral beam heating are inefficient, and when ion cyclotron radiofrequency heating can be difficult to apply due to coupling.

Lloyd has used a zero-dimensional model to assess the need for additional power during start-up for ITER.[28] The electron power balance in this model is given by Eq. (1). P_{OH} and P_{RF} are the ohmic and RF input power, $(P_{Dion} + P_{Drad})$,

$$\frac{3}{2}\frac{d}{dt}(n_e K T_e) = P_{OH} + P_{RF} - (P_{Dion} + P_{Drad}) - P_{e-i} - P^e_{con} - P_{brem} - \sum_I (P_{ion} + P_{line} + P_{RRE} + P_{DRE}) \quad (1)$$

is the power lost to ionization and radiation from deuterium, P_{e-i} is the power flow from the electrons to the ions, P^e_{con} is the heat loss from the electrons due to confinement, P_{brem} is the radiated power due to bremsstrahlung, and the sum over the impurity ions of $(P_{ion} + P_{line} + P_{RRE} + P_{DRE})$ is the power lost due to ionization, line radiation, radiative recombination, and dielectronic recombination of the impurities. The ion power balance is given by

$$\frac{3}{2}\frac{d}{dt}(n_i K T_i) = P_{e-i} - P_{CX} - P^i_{con}, \quad (2)$$

where P_{CX} is the loss due to charge-exchange and P^i_{con} is the heat loss from the ions due to confinement. The particle balance is given by

$$\frac{dn_D}{dt} = \frac{V_n}{V_p} S n_0 n_e - \frac{n_D}{\tau_p}, \quad (3)$$

where n_D, n_0, and n_e are the deuterium, neutral atom, and electron density, respectively, S is the ionization rate, τ_p is the particle confinement time, and (V_n/V_p) is a factor to take into account the fraction of the plasma volume that is accessible to neutrals. The 0-D model handles impurities by assuming they are a fixed fraction of n_D and uses a deuterium recycling coefficient of $R = 1.01$, that is, for each 100 deuterons escaping the plasma to the walls, 101 will return to the plasma as a result of dislodging bound deuterium from the surface. The results of this modeling indicate that burn-through with 2% Be minority should be possible in ITER for low fill densities of $1.5 \times 10^{17}/m^3$ (2×10^{-6} Torr) and a post avalanche density of $<1.5 \times 10^{18}/m^3$, However, for 5% Be or higher fill pressure, failure is likely. If 2 MW of ECRH is used, 5% Be with a post avalanche density of $5 \times 10^{18}/m^3$ can be successful, but not with 2% C. At the same density and 5% C, 5 MW of ECRH is required for robust start-up. ITER has plans for several MW of ECRH power and use of some of that during start-up should be adequate to ensure success.

For normal aspect ratio tokamaks with toroidal fields in the range of about 1 to 4 T, fundamental O-mode (E∥B) and 2nd harmonic X-mode (E⊥B) can access the plasma from low-field-side launch at the appropriate densities as has been reported by Refs. 17, 29, and 30 and references cited therein. The time evolution of ECRH assisted start-up is shown in Figures 5 and 6, which are from 2nd harmonic X-Mode injection on DIII-D.[31] The camera images in Figure 5 show C^{III} emission during the discharge, which forms just inside of the 2nd harmonic resonance layer (a), expands radially (b) and (c), driven by the EXB drift, fills the vessel as the loop voltage is applied and the plasma current increases to form closed flux surfaces (d), the plasma limits on the inner wall (e) and finally is moved to its preprogrammed position, limited on the low field side after 20 ms (f). Figure 6 shows the progression of the plasma during ECRH start-up on DIII-D.[32] As P_{ECH} is increased, the first phase is collisionless heating where the electrons do not gain sufficient energy to ionize the gas, as the power is increased the avalanche occurs and the plasma expands with low I_p. When the toroidal electric field is applied, I_p increases and at about 20 kA, closed flux surfaces form as evidenced by the rapid increase of T_{ECE}, the electron temperature measured by electron cyclotron emission, at −3 ms. Burn-through follows with additional heating from ECRH.

E. Examples from EAST and KSTAR

In general, the start-up phase of discharges gets attention only when there is a failure. Sometimes the failure can be traced rather quickly to some hardware issue but at other times, the cause is not obvious. A couple examples from the start-up of new devices are instructive. During the initial attempts to start-up the EAST tokamak, there were repeated failures with the plasma current never exceeding 35 kA and the discharge ending at 70 to 100 ms. At this early stage of EAST's operation, many of the diagnostics were unavailable. The images of the plasma during the attempted start-up were difficult to interpret because the interior surfaces of EAST

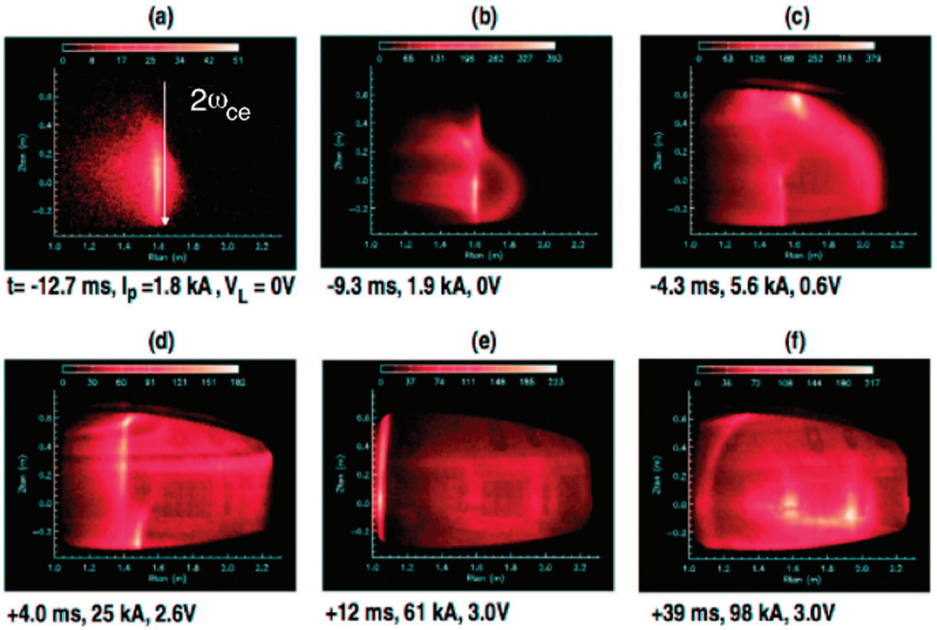

FIG. 5. Fast-framing camera images show the C^{III} emission at various times during the start-up of DIII-D assisted by 2nd harmonic X-Mode ECRH. The caption below each frame shows the time in ms, I_p in kA, and the loop voltage at that time. Reprinted with permission from G. L. Jackson *et al.*, Phys. Plasmas **17**, 056116 (2010). Copyright 2010, American Institute of Physics.

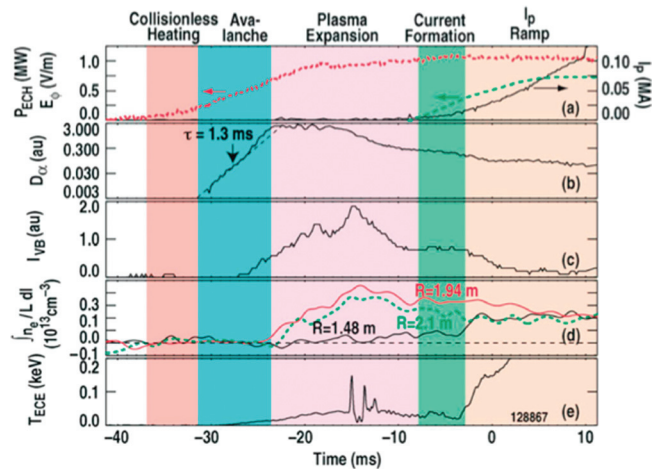

FIG. 6. Phases of plasma evolution with ECRH assisted plasma start-up. The first frame shows the ECH power (red), applied toroidal electric field (green), and I_p (black) versus time. The 2nd and 3rd frames show the D_α emission and intensity of the visible bremsstrahlung, respectively. The 4th frame has the line average density of vertical views at 1.48 m (black), 1.94 m (red), and 2.1 m (green). The bottom frame is the electron temperature measured by electron cyclotron emission. Reprinted with permission from G.L. Jackson *et al.*, Fusion Sci. Technol. **57**, 27 (2010). Copyright 2010 The American Nuclear Society.

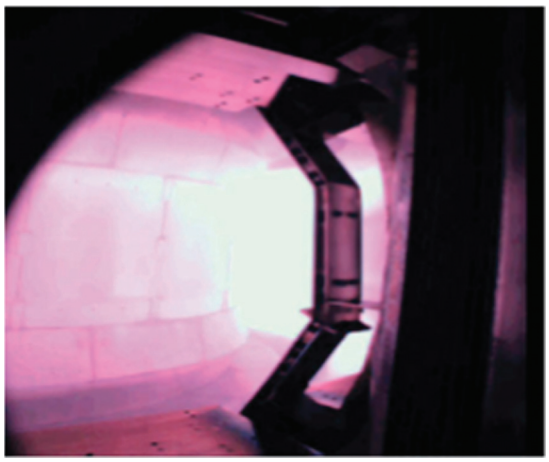

FIG. 7. Fast camera image of plasma in EAST just after breakdown. The bright plasma and metallic surfaces make interpretation of the plasma location uncertain. Reprinted with permission from J. A. Leuer *et al.*, Fusion Sci. Technol. **57**, 48 (2010). Copyright 2010 The American Nuclear Society.

were mostly stainless steel, so there were multiple reflections and no obvious single plasma contact point could be seen as the CCD image in Figure 7 from Ref. 33 illustrates. The obvious candidate for the problem was failure to burn-through low Z impurities. The first attempts at breakdown used an insertable breakdown resistor in all the poloidal field coil circuits for 100 ms to provide additional voltage from the IR drop in the coils that were precharged to positive current. However, the coil currents that were observed did not match that from modeling done prior to operation. In particular, the outer poloidal field (PF) coils which provide the vertical field for plasma radial position control were more positive than the model indicated and differed further from the model later in time. Equation (4) provides an approximate value the vertical field required for radial position control.

$$B_z = -\frac{\mu_0 I_p}{4\pi R_0}\left[\ln\left(\frac{8R_0}{a}\right) + \frac{l_i}{2} + \beta_p - \frac{3}{2}\right]$$
$$\text{where} \quad \beta_p \sim 0.1 \quad \text{and} \quad l_i = \frac{2}{\mu_0^2 R I^2}\int B_p^2 dV \sim 1. \tag{4}$$

When the breakdown resistor time was shortened to 50 ms, the discharge survived and ramped up to about 150 kA on the first attempt. The plasma current did decrease at about 50 ms before the successful ramp-up as can be seen in Figure 8 that shows the first successful EAST plasmas. Further shortening of the resistor time did not result in successful plasmas. This experience emphasizes the need for good modeling of the plasma circuit and power supplies. Since then, the power supplies on EAST have been upgraded to higher voltages for better control.

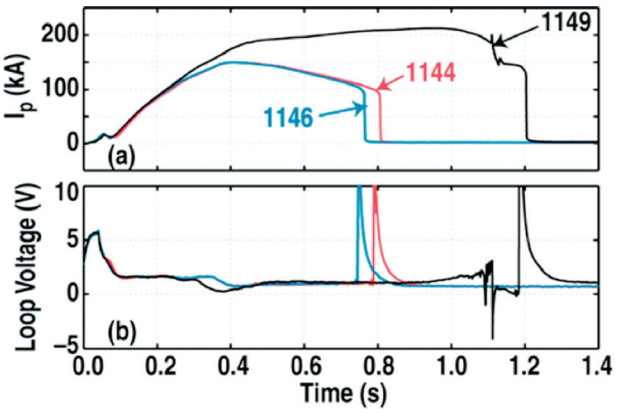

FIG. 8. The first 3 successful discharges on EAST. Note that previous attempts had all resulted in I_p falling from about 35 kA to zero before 0.1 s. Reprinted with permission from J. A. Leuer *et al.*, Fusion Sci. Technol. **57**, 48 (2010). Copyright 2010 The American Nuclear Society.

As the following example from KSTAR illustrates, it is not enough to

$$B_r = -n\frac{B_z}{R_0}[Z - Z_0], \tag{5}$$

$$n = -(R/B_z)(\partial B_z/\partial R) \Rightarrow 0 < n < 3/2, \tag{6}$$

supply the proper vertical field at a single location. The shape of the field must provide stability against motion. The field index, n, given in Eq. (6) must be greater than zero to ensure vertical stability and less that 3/2 to ensure radial stability. KSTAR has ferromagnetic material in its coil jackets,[34] which was chosen for its thermal expansion compatibility. During the first year of KSTAR operation, there was a significant fraction of the discharges that would move onto the inner wall and terminate early and it was not possible to produce a discharge without the use of ECRH assist. An analysis of the field pattern around the time of breakdown by Kim,[35] which included the effects of the ferromagnetic material, indicated that the vertical field near the central column was larger than was indicated by calculations that did not take the ferromagnetic material effect into account. There was a region inside some major radius where $n > 3/2$ and the plasma was radially unstable. This explained the start-up failures. If the initial current channel was formed at too small R, then the plasma was unstable. Without ECRH, the initial plasma had lower current and lower β, so it was formed at a smaller R where $n > 3/2$. When the initial field coil currents were adjusted to compensate for the ferromagnetic effect, it was possible to initiate plasmas without the use of ECRH and the random start-up failures largely disappeared.

F. Electron density during ramp-up

The density during start-up depends upon recycling of gas from the wall. It is a common feature in graphite walls that the density increases with I_p during start-up when the plasma is limited on the graphite surface even without additional gas fueling. In devices with all metal or Be surfaces such as Alcator-C-MOD,[36] ASDEX-U,[25] and JET with the ILW,[27] this increase of n_e with I_p in the absence of additional fueling is not observed. The density behavior during start-up for typical discharges in JET with the ILW is different than that for JET with its graphite wall. For the graphite wall, without gas fueling, the density rises with I_p, while for the ILW, the density falls to very low levels unless additional fueling is provided by means of gas puffing. Gas puffing with the ILW can increase the density to values above those typical of the graphite wall without gas puffing.

G. Current density during ramp-up

The current density profile evolution during ramp-up is influenced in part by T_e that in turn is determined partly by the density evolution. As T_e rises, the rate at which the plasma current is able to penetrate the plasma decreases and this can result in tearing mode instabilities during plasma ramp-up[37] at low l_i. Growing the plasma's aperture size as I_p is increased to keep the $q(a) \sim$ constant during much of the ramp-up allows the current to penetrate and can avoid instabilities.[19] Figure 9 shows a comparison of NSTX discharges grown at about constant q with a large bore throughout the current ramp. The large bore plasma has lower l_i that indicates a broader current profile. The low loop voltage available on ITER necessitates a low I_p ramp rate and allows current to penetrate so that if a constant growth technique were to be used, early sawteeth would be facilitated. Furthermore, the discharge would be in contact with the limiter up to about 15 MA before diverting and this could cause excessive heating of the limiter. Experiments carried out on DIIII-D using a large bore scenario demonstrated less heating of the limiter and l_i closer to the projected ITER target.[38]

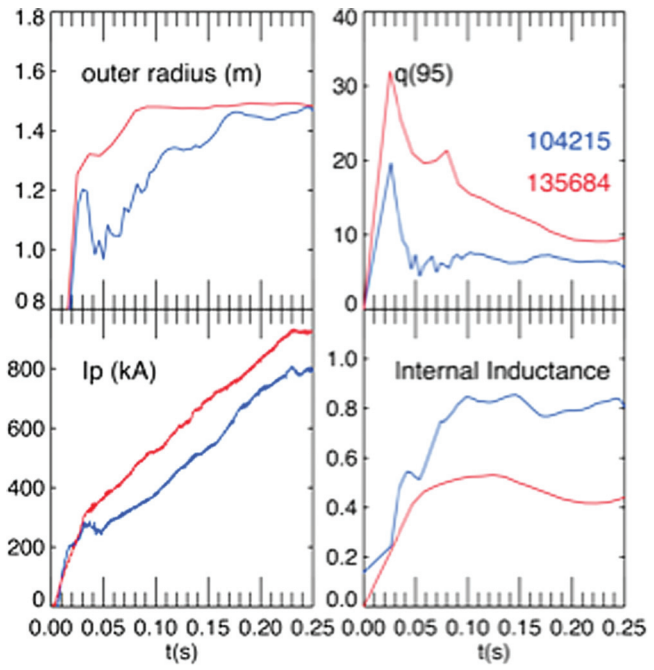

FIG. 9. Comparison of evolution of a discharge initiated with a large-bore (red) with one grown from a smaller aperture (blue) such that q95 reaches its flattop value early and approximately constant after 0.05 s. Note that the factor of two difference in internal inductance (l_i) at the start of plasma current flattop.

H. Plasma start-up without a solenoid

Use of a central solenoid both works reliably and is well understood, but there are reasons to consider other start-up strategies: In particular, elimination of the central solenoid is required to achieve low aspect ratio at small device size for fusion nuclear applications. If non-inductive current drive could support a steady state reactor, an alternative start-up technique would allow elimination of the solenoid, and with a reduced size or no central solenoid, the cost and size of a conventional tokamak reactor could be reduced. Inductive techniques that do not rely upon a central solenoid must address all the same physics issues, but the emphasis may differ. For example, use of an iron core in place if an air-cored solenoid can avoid engineering issues caused by neutron damage to insulation in the central solenoid of a reactor, but requires engineering design of the system to be carried out.[39] The outer poloidal field coils can be used to provide both loop voltage and flux to start-up the plasma and has been demonstrated on JT-60[8] and DIII-D[9]. Providing a good field null and a stabilizing poloidal field while providing flux by ramping the coils to finally provide a diverted plasma shape at high plasma current capable of being sustained by other means must address all the physics issues of inductive breakdown through controlled plasma current ramp-up.[40]

III. START-UP USING RF WAVES

Lower Hybrid Current Drive (LHCD) start-up to 100 kA was demonstrated on PLT,[41] and ECRH was used to provide start-up to low current levels on DIII-D,[42] TS2,[43] and LATE.[44] For the ST, however, Electron-Bernstein Wave (EBW) seems most promising.[45] This technique has produced I_p of 33 kA with only 100 kW of ECRH on MAST.[10,46] The EBW is an electrostatic wave that can exist only in a plasma so it cannot be launched directly by an antenna outside the plasma, but it can be produced by mode-conversion at the upper hybrid resonance (UHR) layer of X-Mode ECRH waves launched from the high-field side (HFS).[47] The UHR frequency is $\omega_{UH} = (\omega_p^2 + \omega_{ce}^2)^{1/2}$ where $\omega_{ce} = eB/m_e$ and $\omega_p = (n_e e^2/\varepsilon_0 m_e)^{1/2}$. Because access to the HFS is difficult in an ST, the MAST solution is to launch O-Mode ECRH at 28 GHz from the low field side. The O-Mode wave is not strongly damped below the density cutoff of $1 \times 10^{19}/m^3$. A grooved polarizing mirror cut into the central column converts the O-Mode to X-Mode. The geometry and results of ray-tracing modeling for MAST are shown in Figure 10. The O-Mode is launched from below the midplane so the beam reflected at the midplane is largely above the midplane as it propagates outward in the plasma. As the outgoing X-Mode wave approaches the UHR, its index of refraction, n, increases, it slows, is mode converted to an EBW reflected perpendicular to the UHR. The sign of the refractive index in the direction parallel to the magnetic field, $n_{||}$, is determined by the direction of the projection of wave vector k along the poloidal field and it is the sign of $n_{||}$ that determines if the EBW will accelerate electrons parallel or anti-parallel to the toroidal field when it is absorbed at the electron cyclotron resonance. Because the poloidal field changes sign when closed flux forms, the direction of the EBW current driven above or below the midplane changes. MAST has exploited that by using the radial field to shift the plasma's midplane above the machine's midplane such that the EBW mostly propagates below the plasma's midplane and thus drives mostly co-directed current before closed flux forms and then shifting the plasma down when closed flux forms and the direction of $n_{||}$ changes. The result of making such a well-orchestrated timing of the radial field to produce a vertical shift when the formation of closed flux surfaces appears is illustrated in Figure 11 for two different vertical field programs. Extrapolation of these results from MAST indicates start-up current per launched power of 0.33 MA/MW.

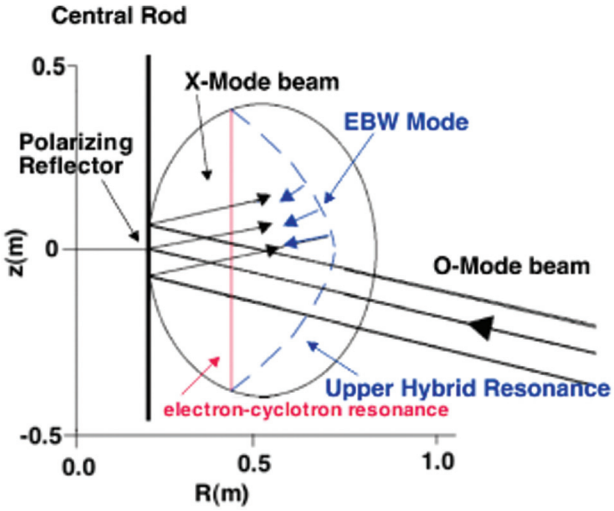

FIG. 10. Results of ray-tracing done for EBW on MAST. Note that because the incoming O-Mode ECH beam is launched from below the midplane towards the polarizing reflector at the midplane, the outgoing X-Mode ECH is mostly above the device's midplane. This vertical imbalance is exploited to produce co-current drive as described in the text.

IV. START-UP USING HELICITY INJECTION

The concept of magnetic helicity, which is given by $K = \int \vec{A} \cdot \vec{B} dv$ where $\vec{A}$ is the vector potential, $\vec{B}$ is the magnetic field, and v is the plasma volume can be used to describe current drive in a tokamak.[48] Plasma start-up by helicity injection as well as coupling to inductive sustainment has been successfully demonstrated by both transient coaxial helicity injection (CHI)[49,50] and by point source helicity injection from plasma guns.[51]

A. Helicity injection from plasma guns

Plasma guns have been employed on PEGASUS to inject helicity and provide start-up plasmas that can be coupled to inductive ramp-up.[52] The gun location is flexible, and the guns could be withdrawn after start-up and do not provide an obvious impurity source to the plasma. All these are potential advantages of the use of the guns for start-up. The scaling of I_p from helicity injection is not simple since it arises from considering two limits.[47] One is the relaxation limit that arises from consideration of the Taylor minimum energy state. The scalar representing the average inverse scale length of the helical magnetic field is $\lambda_T = \mu_0 I_p/\Psi_T$ and $\lambda_{inj} = \mu_0 I_{inj}/\Psi_{edge}$ in the plasma volume and in the

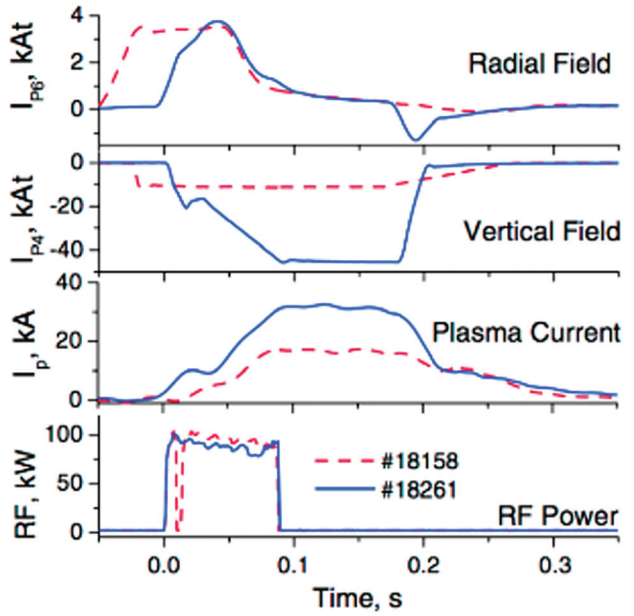

FIG. 11. The radial field in MAST is used to move the plasma centroid up before closed flux surfaces are formed so that so the majority of the X-Mode ECH and EBW are below the plasma midplane and produces co-current drive. Moving the plasma down as I_p increases to form closed flux puts the EBW above the plasma midplane and produces co-current drive. The red-dashed curve with constant vertical field demonstrates that the current is not driven by flux from the vertical field. The blue curves indicate a case with the vertical field increased as I_p is increased to maintain better position control. Reprinted with permission from V. F. Shevchenko *et al.*, Nucl. Fusion **50**, 022004 (2010).

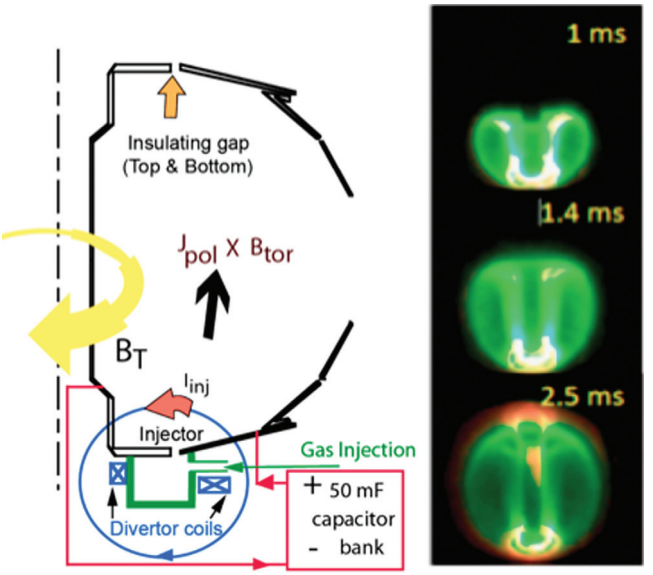

FIG. 12. The main components of the NSTX CHI system discussed in the text. The fast, color camera images on the right show the plasma growing into the vessel in time. The green color is due to Li emission.

injector regions, respectively, where $\Psi_T = B_T A_p$ and $\Psi_{edge} = 2\pi R_{edge} w B_{z,edge}$. $B_{z,edge}$ is due to both I_p and the vacuum field. Relaxation drives current from higher to lower λ and this results in

$$I_p \leq f_{Geom}\left(\frac{\varepsilon A_p I_{inj} I_{TF}}{2\pi R_{edge} w}\right)^{1/2}, \quad (7)$$

where $1 < f_{\mathrm{Geom}} < 3$ is a factor that depends upon geometry. The I_p limit in Eq. (7) indicates I_p scales with injector properties like the square root of the gun current and inversely as the square root of the source width. A second scaling arises from the helicity input rate and implies that I_p driven by helicity from the injector scales directly with the area of the gun source and the gun bias voltage. Thus, the scaling of I_p will depend upon the toroidal field, the gun impedance, and the geometry. Results from PEGASUS have demonstrated the ramp-up of an 80 kA plasma initiated by plasma guns to 150 kA inductively.[50]

B. Coaxial helicity injection (CHI)

Implementation of transient CHI on NSTX is accomplished through series of actions described below. The sketch in Figure 12 shows the important components for transient CHI. The vacuum vessel is separated electrically by insulating gaps at the top and bottom of the machine. The toroidal field is applied and the lower divertor coils are used to produce a poloidal field that connects the inner and outer vessels. Deuterium gas is injected at the bottom and 1.65 kV is applied from a variable (5 to 50 mF) capacitor bank across the insulating gap. Breakdown proceeds, again via a Townsend avalanche along the helical field connecting inner and outer vessel. Since the toroidal field is much stronger than the initial poloidal field, each field line wraps many times around the major axis while connecting the inner and outer electrodes so the toroidal current can be tens to hundreds of times the injector current (I_{inj}) between the electrodes. The direction of the $J_{pol}X\ B_T$ is up into the vacuum vessel. When $I_{inj} > 2\ \psi_{inj}^2/(\mu_0^2 d^2 I_{TF})$, where ψ_{inj} is the flux connecting the inner and outer vessels, d is the separation of the flux footprint, and I_{TF} is the total toroidal current in the center column,[53] the plasma rapidly expands to fill the vessel as can be seen by the three fast camera images at 1, 1.4, and 2.5 ms. The capacitor voltage driving the injected current is then removed by a fast acting crowbar switch. This forces reconnection of the field lines and when $I_{inj} = 0$, all the toroidal current is flowing on closed flux surfaces. Similar to Eq. (7), it can be shown, using the inverse scale lengths for the helical magnetic field and the equation for the injector current that the CHI produced plasma current is directly proportional to the injector flux that connects the lower divertor plates.

$$I_P \leq 2\psi_T \psi_{inj}/(\mu_0^2 d^2 I_{TF}). \quad (8)$$

Since it begins as an electrode discharge, potential difficulties with CHI are that impurities from the electrode surfaces, low T_e, or unsuitably high n_e may render the CHI formed plasma unsuitable for start-up of a tokamak discharge. These considerations have been addressed experimentally[54,55] and as can be seen in Figure 13, discharges that are initiated with transient CHI can be coupled to inductive ramp-up. In this example, the CHI initiated plasmas have $I_p > 300$ kA greater than those formed with inductive start-up using the same inductive flux.

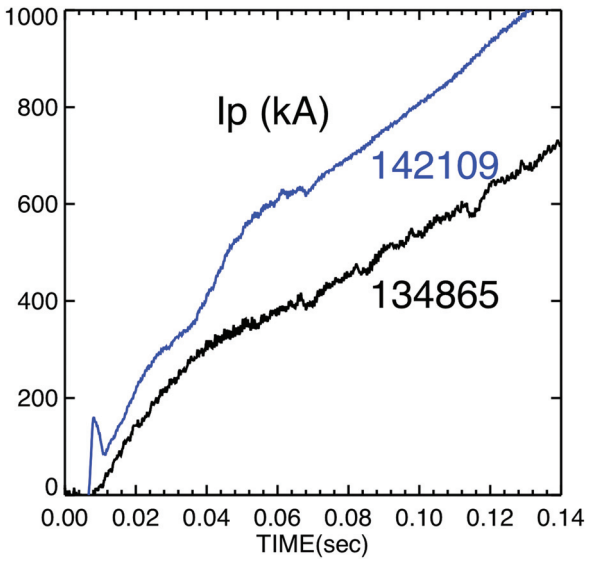

FIG. 13. The plasma current in kA for a discharge initiated with CHI and further ramped with induction (blue) is compared to a reference inductive-only discharge from the NSTX 10YR data base that reached 1 MA in a shorter time than other discharges (black). At 120 ms, the solenoid flux used by both discharges is the same.

V. SUMMARY

Inductive start-up is well understood. The Townsend avalanche and impurity burn-through have been modeled self-consistently. With ECRH assist, inductive startup should serve to produce high current plasmas in ITER and JT-60SA. However, future spherical tokamaks with nuclear capability will have little space for a central solenoid, which makes the usual inductive technique problematic, although the use of an unshielded iron core could provide some initial current. Outer PF induction, EBW, CHI, and point source helicity injection are possible alternatives for start-up on ST reactors. Each of these techniques demonstrated start-up to significant current. Experiments on present devices will provide scaling to higher plasma current and refine the choices available for future ST reactors.

ACKNOWLEDGMENTS

I would like to thank Gary Jackson, Peter deVries, Vladimir Schevchenko, Gary Taylor, Michael Bell, Roger Raman, Devon Battaglia, Walter Guttenfelder, David Gates, and Jon Menard for valuable discussions and for sharing the results of their research with me. This work was supported by U.S. DOE Contract No. DE-AC02-09CH11466.

This manuscript has been authored by Princeton University and collaborators under Contract No. DEAC0209CH11466 with the U.S. Department of Energy. The publisher, by accepting the article for publication, acknowledges that the United States Government retains a nonexclusive, paidup, irrevocable, worldwide license to publish or reproduce the published form of this manuscript, allow others to do so, for United States Government purposes.

[1]B. Wan, Plasma Sci. Technol. **9**, 125 (2007).
[2]Y.-K. Oh, W. C. Kim, K. R. Park, M. K. Park, H. L. Yang, Y. S. Kim, Y. Chu, Y. O. Kim, J. G. Bak, E. N. Baang, S. W. Yoon, S. H. Hahn, H. J. Lee, S. H. Park, K. H. Kim, J. Hong, S. H. Baek, M. K. Kim, T. G. Lee, S. I. Lee, Y. S. Bae, H. Yonekawa, J. H. Choi, I. S. Hwang, Y. J. Kim, K. W. Cho, Y. M. Park, J. Y. Kim, J. H. Lee, J. S. Bak, M. Kwon, G. S. Lee, J. G. Kwak, H. S. Ahn, M. L. Walker, D. A. Humphreys, J. A. Leuer, A. Hyatt, G. Jackson, D. Mueller, and D. P. Ivanov, Fusion Eng. Des. **84**, 344 (2009).
[3]P. H. Rebut, R. J. Bickerton, and B. E. Keen, Nucl. Fusion **25**, 1011 (1985).
[4]G. F. Matthews, P. Coad, H. Greuner, M. Hill, T. Hirai, J. Likonen, H. Maier, M. Mayer, R. Neu, V. Philipps, R. Pitts, and V. Riccardo, J. Nucl. Mater. **390**, 934 (2009).
[5]J. E. Menard, S. Gerhardt, M. Bell, J. Bialek, A. Brooks, J. Canik, J. Chrzanowski, M. Denault, L. Dudek, D. A. Gates, N. Gorelenkov, W. Guttenfelder, R. Hatcher, J. Hosea, R. Kaita, S. Kaye, C. Kessel, E. Kolemen, H. Kugel, R. Maingi, M. Mardenfeld, D. Mueller, B. Nelson, C. Neumeyer, M. Ono, E. Perry, R. Ramakrishnan, R. Raman, Y. Ren, S. Sabbagh, M. Smith, V. Soukhanovskii, T. Stevenson, R. Strykowsky, D. Stutman, G. Taylor, P. Titus, K. Tresemer, K. Tritz, M. Viola, M. Williams, R. Woolley, H. Yuh, H. Zhang, Y. Zhai, A. Zolfaghari, and NSTX Team, Nucl. Fusion **52**, 083015 (2012).
[6]N. Hosogane, JT-60SA Design Team, and Japan-Europe Satellite Tokamak Working Group, Fusion Sci. Technol. **52**, 375 (2007).
[7]M. Shimada, D. J. Campbell, V. Mukhovatov, M. Fujiwara, N. Kirneva, K. Lackner, M. Nagami, V. D. Pustovitov, N. Uckan, J. Wesley, N. Asakura, A. E. Costley, A. J. H. Donné, E. J. Doyle, A. Fasoli, C. Gormezano, Y. Gribov, O. Gruber, T. C. Hender, W. Houlberg, S. Ide, Y. Kamada, A. Leonard, B. Lipschultz, A. Loarte, K. Miyamoto, V. Mukhovatov, T. H. Osborne, A. Polevoi, and A. C. C. Sips, Nucl. Fusion **47**, S1 (2007).
[8]M. Ushigome, S. Ide1, S. Itoh, E. Jotaki, O. Mitarai, S. Shiraiwa, T. Suzuki, Y. Takase, S. Tanaka, T. Fujita, P. Gohil, Y. Kamada1, L. Lao, T. Luce, Y. Miura, O. Naito, T. Ozeki, P. Politzer, Y. Sakamoto, and JT-60 Team, Nucl. Fusion **46**, 207 (2006).
[9]J. A. Leuer, G. Cunningham, D. Mueller, N. H. Brooks, N. W. Eidietis, D. A. Humphreys, A. W. Hyatt, G. L. Jackson, J. Lohr, P. A. Politzer, R. I. Pinsker, R. Prater, P. L. Taylor, M. L. Walker, R. V. Budny, D. A. Gates, A. Nagy, S.-H. Hahn, Y.-K. Oh, S.-W. Yoon, J. H. Yu, M. Murakami, J. M. Park, and A. C. Sontag, Nucl. Fusion **51**, 063038 (2011).
[10]V. F. Shevchenko1, M. R. O'Brien1, D. Taylor *et al.*, Nucl. Fusion **50**, 022004 (2010).
[11]B. A. Nelson, T. R. Jarboe, A. K. Martin, D. J. Orvis, J. Xie, C. Zhang, and L. Zhou, Phys. Plasmas **2**, 2337 (1995).
[12]N. W. Eidietis, R. J. Fonck, G. D. Garstka, E. A. Unterberg, and G. R. Winz, J. Fusion Energy **26**, 43 (2007).
[13]M. Gryzinski, Phys. Rev. **138**, A305, A322, A336 (1965).
[14]J. S. Townsend, *Electricity in Gases* (Clarendon Press, Oxford, 1915).
[15]S. C. Brown, *Introduction to Electrical Discharges in Gases* (John Wiley and Sons, 1966).
[16]F. Paschen, Ann. Phys. **273**(5), 69 (1989); M. A. Lieberman and A. J. Lichtenberg, *Principles of Plasma Discharges and Materials Processing* (John Wiley & Sons Inc., Hoboken, NJ, 2005).
[17]B. Lloyd, G. L. Jackson, T. S. Taylor, E. A. Lazarus, T. C. Luce, and R. Prater, Nucl. Fusion **31**, 2031 (1991).
[18]R. Papoular, Nucl. Fusion **16**, 37 (1976).
[19]A. Tanga, P. R. Thomas, J. G. Cordey, J. P. Christiansen, S. Ejima, A. Kellman, E. Lazzaro, P. J. Lomas, P. Morgan, F. Nave, P. Noll, and F. C. Schuller, in *Tokamak Start-up*, edited by H. Knoepfel (Plenum Press, NY, 1985).
[20]D. E. Post, R. V. Jensen, C. B. Tarter, W. H. Grasberger, and W. A. Lokke, At. Data Nucl. Data Tables **20**, 397 (1977).
[21]A. E. Pontau and D. H. Morse, J. Nucl. Mater. **141–143**, 124 (1986).
[22]G. L. Jackson, T. S. Taylor, and P. L. Taylor, Nucl. Fusion **30**, 2305 (1990).
[23]J. Winter, H. G. Esser, L. Könen, V. Philipps, H. Reimer, J. v. Seggern, J. Schlüter, E. Vietzke, F. Waelbroeck, P. Wienhold, T. Banno, D. Ringer, and S. Vepřek, J. Nucl. Mater. **162–164**, 713 (1989).
[24]H. W. Kugel, M. G. Bell, J.-W. Ahn, J. P. Allain, R. Bell, J. Boedo, C. Bush, D. Gates, T. Gray, S. Kaye, R. Kaita, B. LeBlanc, R. Maingi, R. Majeski, D. Mansfield, J. Menard, D. Mueller, M. Ono, S. Paul, R. Raman, A. L. Roquemore, P. W. Ross, S. Sabbagh, H. Schneider, C. H. Skinner, V. Soukhanovskii, T. Stevenson, J. Timberlake, W. R. Wampler, and L. Zakharov, Phys. Plasmas **15**, 056118 (2008).
[25]R. L. Neu, IEEE Trans. Plasma Sci. **38**(3), 454 (2010).
[26]H.-T. Kim, W. Fundamenski, A. C. C. Sips, and EFDA-JET Contributors, Nucl. Fusion **52**, 103016 (2012).

[27]P. C. de Vries *et al*., "Comparison of plasma breakdown with a carbon and ITER-like wall," Nucl. Fusion (submitted); P. C. de Vries, P. J. Lomas, F. Maviglia, R. Albanese, I. Coffey, E. Joffrin, M. Lehnen, A. Manzanares, M. O'Mulane, I. Nunes, G. van Rooij, F. G. Rimini, M. F. Stamp, and JET-EFDA Contributors, in 25th IAEA, SanDiego, EXD4-2, 2012.
[28]B. Lloyd, P. G. Carolan, and C. D. Warric, Plasma Phys. Controlled Fusion **38**, 1627 (1996).
[29]G. L. Jackson, J. S. deGrassie, C. P. Moeller, and R. Prater, Nucl. Fusion **47**, 257 (2007).
[30]K. Kajiwara, Y. Ikeda, M. Seki, S. Moriyama, T. Oikawa, T. Fujii, and JT-60 Team, Nucl. Fusion **45**, 694 (2005).
[31]G. L. Jackson, P. A. Politzer, D. A. Humphreys, T. A. Casper, A. W. Hyatt, J. A. Leuer, J. Lohr, T. C. Luce, M. A. Van Zeeland, and J. H. Yu, Phys. Plasmas **17**, 056116 (2010).
[32]G. L. Jackson, M. E. Austin, J. S. de Grassie, A. W. Hyatt, J. M. Lohr, T. C. Luce, R. Prater, and W. P. West, Fusion Sci. Technol. **57**, 27 (2010).
[33]J. A. Leuer, B. J. Xiao, D. A. Humphreys, M. L. Walker, A. W. Hyatt, G. L. Jackson, D. Mueller, B. G. Penaflor, D. A. Piglowski, R. D. Johnson, A. S. Welander, Q. P. Yuan, H. Z. Wang, J. R. Luo, and EAST Team, Fusion Sci. Technol. **57**, 48 (2010).
[34]H. Yonekawa, Y. O. Kim, H. J. Lee, S. W. Yoon, S. Hahn, K. S. Lee *et al*., IEEE Trans. Appl. Supercond. **19**, 1573–1576 (2009).
[35]J. Kim, S. W. Yoon, Y. M. Jeon, J. A. Leuer, N. W. Eidietis, D. Mueller, S. Park, Y. U. Nam, J. Chung, K. D. Lee, S. H. Hahn, Y. S. Bae, W. C. Kim, Y. K. Oh, H. L. Yang, K. R. Park, H. K. Na, and KSTAR Team, Nucl. Fusion **51**, 083034 (2011).
[36]I. H. Hutchinson, R. Boivin, F. Bombarda, P. Bonoli, S. Fairfax, C. Fiore, J. Goetz, S. Golovato, R. Granetz, M. Greenwald, S. Horne, A. Hubbard, J. Irby, B. LaBombard, B. Lipschultz, E. Marmar, G. McCracken, M. Porkolab, J. Rice, J. Snipes, Y. Takase, J. Terry, S. Wolfe, C. Christensen, D. Garnier, M. Graf, T. Hsu, T. Luke, M. May, A. Niemczewski, G. Tinios, J. Schachter, and J. Urbahn, Phys. Plasmas **1**, 1511 (1994).
[37]J. Wesson, R. D. Gill, M. Hugonet, J. A. Snipes, D. J. Ward, D. V. Bartlett, D. J. Campbell, P. A. Duperrex, A. W. Edwards, R. S. Granetz, N. A. O. Gottardi, T. C. Hender, E. Lazzaro, P. J. Lomas, N. Lopes Cardozo, K. F. Mast, M. F. F. Nave, N. A. Salmon, P. Smeulders, P. R. Thomas, B. J. D. Tubbing, M. F. Turner, and A. Weller, Nucl. Fusion **29**, 641 (1989).
[38]G. Jackson, T. A. Casper, T. C. Luce, D. A. Humphreys, J. R. Ferron, A. W. Hyatt, E. A. Lazarus, R. A. Moyer, T. W. Petrie, D. L. Rudakov, and W. P. West, Nucl. Fusion **48**, 125002 (2008).
[39]D. A. Gates, C. Jun, I. Zatz, and A. Zolfaghari, Fusion Eng. Des. **86**, 41 (2011).
[40]W. Choe, J. Kim, and M. Ono, Nucl. Fusion **45**, 1463 (2005).
[41]F. Jobes, J. Stevens, R. Bell, S. Bernabei, A. Cavallo, T. K. Chu, S. Cohen, B. Denne, P. Efthimion, E. Hinnov, W. Hooke, J. Hosea, E. Mazzucato, R. McWilliams, R. Motley, S. Suckewer, G. Taylor, J. Timberlake, S. von Goeler, and R. Wilson, Phys. Rev. Lett. **52**(12), 1005 (1984); C. F. F. Karney, N. J. Fisch, and F. C. Jobes, Phys. Rev. A **32**, 2554–2556 (1985); N. J. Fisch, Rev. Mod. Phys. **59**, 175–234 (1987).
[42]G. L. Jackson, D. A. Humphreys, A. W. Hyatt, J. M. Lohr, T. C. Luce, and J. H. Yu, Nucl. Fusion **51**, 083015 (2011).
[43]A. Ejiri, Y. Takase, H. Kasaharaet, T. Yamada, K. Hanada, K. N. Sato, H. Zushi, K. Nakamura, M. Sakamoto, H. Idei, M. Hasegawa, A. Iyomasa, N. Imamura, K. Esaki, M. Kitaguchi, K. Sasaki, H. Hoshika, O. Mitarai, and N. Nishino, Nucl. Fusion **46**, 709 (2006).
[44]T. Yoshinaga, M. Uchida, H. Tanaka, and T. Maekawa, Phys. Rev. Lett. **96**, 125005 (2006).
[45]A. Montes and G. O. Ludwig, Plasma Phys. Controlled Fusion **28**, 1765 (I986).
[46]V. Shevchenko, in *EC-15 Joint Workshop, Yosemite, CA, USA* (2008).
[47]H. P. Laqua, Plasma Phys. Controlled Fusion **49**, R1 (2007).
[48]D. J. Battaglia, M. W. Bongard, R. J. Fonck, and A. J. Redd, Nucl. Fusion **51**, 073029 (2011).
[49]R. Raman, T. R. Jarboe, W. T. Hamp, A. J. Redd, B. A. Nelson, R. G. O'Neill, P. E. Sieck, and R. J. Smith, Phys. Plasmas **14**, 022504 (2007).
[50]R. Raman, T. R. Jarboe1, D. Mueller, B. A. Nelson, M. G. Bell, R. Bell, D. Gates, S. Gerhardt, J. Hosea, R. Kaita, H. Kugel, B. LeBlanc, R. Maingi, R. Maqueda, J. Menard, M. Nagata, M. Ono, S. Paul, L. Roquemore, S. Sabbagh, V. Soukhanovskii, and G. Taylor, Nucl. Fusion **49**, 065006 (2009).
[51]D. J. Battaglia, M. W. Bongard, R. J. Fonck, A. J. Redd, and A. C. Sontag, Phys. Rev. Lett. **102**, 225003 (2009).
[52]D. J. Battaglia, J. Fusion Energy **28**, 140 (2009).
[53]T. R. Jarboe, Fusion Technol. **15**, 7 (1989).
[54]B. A. Nelson, T. R. Jarboe, D. Mueller, B. A. Nelson, M. G. Bell, M. Ono, T. Bigelow, R. Kaita, B. LeBlanc, R. Maqueda, J. Menard, S. Paul, L. Roquemore, and NSTX Research Team, Nucl. Fusion **51**, 063008 (2011).
[55]D. Mueller, M. G. Bell, R. Bell, B. P. Benoit, A. L. Roquemore, R. Raman, T. R. Jarboe, B. A. Nelson, S. A. Sabbagh, and V. Soukanovskii, IEEE Trans. Plasma Sci. **38**, 371 (2010).